INTRACOCHLEAR DUCT MECHANICS OF DEVELOPING CHICKEN EMBRYOS

A Thesis

by

KRISTEN MARIE STROMSODT

Submitted to the Jackson College of Graduate Studies of the
University of Central Oklahoma
in partial fulfillment of the requirements for the degree of

MASTER OF SCIENCE

Chair of Committee,	Scott P. Mattison
Committee Members,	Mohammed Bingabr
	Gang Xu
Chair of Department,	Charles Hughes

May 2020

Major Subject: Engineering Physics-Biomedical Engineering

INTRACOCHLEAR DUCT MECHANICS OF DEVELOPING CHICKEN EMBRYOS

Thesis Title

Kristen Stromsodt

Author's Name

4/28/2020

Date

Jackson College of Graduate Studies at the University of Central Oklahoma

A THESIS APPROVED FOR

Master of Science- Biomedical Engineering

By

Scott P. Mattison Digitally signed by Scott P. Mattison Date: 2020.05.08 06:54:11 -05'00'

Committee Chairperson

Gang Xu Digitally signed by Gang Xu DN: cn=Gang Xu, o, ou, email=gxu@uco.edu, c=US Date: 2020.05.08 14:28:29 -05'00'

Committee Member

Mohamed Bingabr Digitally signed by Mohamed Bingabr Date: 2020.05.08 14:56:09 -05'00'

Committee Member

ABSTRACT

The cochlea is a small, coiled part of the inner ear responsible for the transduction of mechanical sound pressure into electrical stimulation in the brain. Despite the importance of the cochlea for normal hearing, the complex mechanical interactions between active and passive components are not well understood. By utilizing a technique known as optical coherence vibrometry, we performed initial quantification of the changes in mechanical motion of the embryonic avian cochlear duct. By quantifying changes in the mechanical response of the cochlea to sound, as key regions of the cochlea develop, we hope to determine the passive role each of these components play in healthy hearing. To quantify the mechanical motion of the cochlea, we exposed the cochlea to pure tone auditory stimuli at various sound pressure levels and frequencies. We recorded the amplitude and phase of the mechanical response of key structures in the cochlea and compared them across developmental stages.

DEDICATION

This thesis is dedicated to my parents Wayne and Sharon Stromsodt and my sister Kayla, for their unwavering support and love during my entire collegiate career.

ACKNOWLEDGEMENTS

First and foremost, I would like to express tremendous amount of gratitude to my thesis supervisor/committee chair, Dr. Scott Mattison, and committee members Dr. Mohamed Bingabr and Dr. Gang Xu. Without their support and guidance this thesis would never have come to fruition. Thank you to my parents, Wayne and Sharon Stromsodt, and my sister, Kayla Stromsodt, who offered a hand to help, a warm hug, or a word of encouragement whenever necessary. I truly could not have completed this without the three of you by my side each and every day. I would also like to thank the rest of my family including aunts Pam Lautt, Judi Whitmore, and Jeanine Deterding and cousin Amber Lautt for all being rocks of unfailing support at all hours, day and night. I would like to thank my best friend, Katie Boettcher, who always knew what to say to ease my nerves and sent care packages to keep me awake on long nights. Thank you to my friends, department faculty, and staff at the University of Central Oklahoma, without whom, this journey would not have been the fantastic and humbling experience it turned out to be.

Lastly, I would like to thank the Lord for giving me the strength and guidance to keep pushing through the difficult times. His wisdom and grace kept me focused on the end goal and gave me the determination to keep researching and finding answers to seemingly impossible questions.

I can do all things through Christ who strengthens me. Philippians 4:13

CONTRIBUTORS AND FUNDING SOURCES

Contributors

This work was supervised by a thesis committee consisting of Dr. Scott Mattison [Advisor], Dr. Mohamed Bingabr and Dr. Gang Xu of the Department of Engineering and Physics at the University of Central Oklahoma.

Funding Sources

This research was funded by the OK-INBRE and UCO RCSA grants.

NOMENCLATURE

OCT	Optical Coherence Tomography
OCV	Optical Coherence Vibrometry
TDOCT	Time Domain Optical Coherence Tomography
SDOCT	Spectral Domain Optical Coherence Tomography
BM	Basilar Membrane
TM	Tectorial Membrane
HC	Hair Cells
SC	Supporting Cells
THC	Tall Hair Cells
SHC	Short Hair Cells
SPL	Sound Pressure Levels

Table of Contents

LIST OF FIGURES

CHAPTER 1-INTRODUCTION

1.1 Purpose of Study

Humans have five primary senses: sight, smell, taste, touch, and hearing. These senses are gifts we all take for granted, until we lose them. Around the world there are more than 460 million people who suffer from some degree of hearing loss. Approximately 48 million of those individuals are Americans[1]. Hearing is a complex pathway involving many interconnected mechanical structures and autonomic responses, eventually leading to the conversion of mechanical sound pressures being converted into neural signals in the cochlea and then sent on to the brain[2]. If any portion of this hearing pathway is damaged, there is a loss of efficacy when transducing these mechanical eaves to electrical stimuli. The cochlea, a part of the inner ear, houses the small soft tissue organ responsible for transduction of sound. Damage to the hearing organ, known as the organ of Corti in mammals, leads to significant hearing loss in patients. There are various pathologies of the inner ear, including: Meniere's disease, viral or bacterial infections, trauma to the ear, or age- related hearing loss[3]. Despite the importance of the cochlea for normal hearing, the mechanical interactions between various components is not well understood. More answers on how the cochlea operates would help doctors develop more treatment options for patients with cochlear damage.

One current treatment for hearing loss is a hearing aid. In 2016 alone, more than 3.65 million hearing aids were dispensed in the United States. The price for one hearing aid can range from $1,000 to $4,000, depending on the level of technology they contain[4]. Most hearing aids are a simple sound amplification that makes the surrounding sounds louder to the patient. They do not create a better quality, clearer sound.

Due to the scale and location of the cochlea, the inability to acquire mechanical measurements of the healthy inner ear during sound transduction has presented a significant barrier to the study of hearing loss. Recent studies have demonstrated the use of a newer technique, optical coherence vibrometry (OCV), to acquire measurements of the mechanical responses of the intact inner ear[5][6]. OCV is capable of imaging picometer scale vibrations of the soft tissue layers of the inner ear through the bony shell of the cochlea. We hypothesize that by using OCV we can quantify the intracochlear duct mechanics of an avian embryo at different stages of development. The research question is as follows: Are there quantifiable changes in the mechanical interactions between various components of the avian duct during the development of the tonotopic pattern of avian hair cells? Hair cells are believed to have key roles in the transduction of sound in the mammalian cochlea. As avian cochleae have been demonstrated to lack active amplification of sound, this study will provide key insight into the passive role these structures may play[7].

1.4 Definitions

1.4.1 Optical Coherence Tomography

Optical Coherence Tomography (OCT) is a non-invasive imaging technique that uses low-coherence interferometry to capture micrometer-resolution two and three-dimensional images from within optical scattering media. OCT benefits from decoupled lateral and axial resolutions to acquire depth dependent images of layered tissue structures.

1.4.2 Optical Coherence Vibrometry

Optical Coherence Vibrometry (OCV) is an extension of OCT which takes advantage of the interferometric nature of OCT to acquire phase sensitive measurements of tissue motion. Properly processed, these measurements provide valuable information for investigating either the mechanical properties or the physiological function of biological tissues, especially in the

hearing organs[8]. OCV has been demonstrated to be especially useful for discerning vibrational motion of layered samples with sensitivity down to the picometer scale. With proper hardware, an image can be acquired in real time and images can be compared to extract movements in nanometers.

1.5 Delimitations, Limitations, and Assumptions

Recent studies in OCV have demonstrated complex non-linear interactions involved in frequency mixing in the cochlea of gerbils and guinea pigs[9][10][11]. Our studies focus solely on pure-tone audiometry. Therefore, we are not probing the role of passive mechanics in the formation of these complex interactions. In addition, this study ignores any potential for active motion by motoring the cochlear mechanics of non-viable chick embryos.

CHAPTER 2-LITERATURE REVIEW

2.1 Anatomy and Development of a Chicken Cochlea

The chicken embryo is a notable system for studying morphogenic events because of its early accessibility and response to manipulation[12]. In addition, the chicken has been demonstrated to distinctly lack the active mechanical motion found in mammalian tissue. Instead the mechanical response to auditory stimulation is passive[7][13][14]. This allows us to explore anatomical structures without the added complexity of active gain. Similar to humans, hearing in the chicken works by entering the ear as a sound wave and is converted to a neural signal via mechanotransduction[15].

The ear develops from the otic capsule which invaginates to form the otocyst. This otocyst gives rise to all membranous components of the inner ear[12]. The inner ear contains three vestibular semicircular canals: the saccule, the utricle, and the cochlear duct[12]. The saccule responds to movements in the vertical plane (up-down) and forward-backward movements in the sagittal plane. The utricle responds to head movements in the horizontal plane such as sideways, head tilts, and rapid lateral displacements[16]. The cochlear duct is distinct from the mammalian cochlea. Instead of being the small, snail shell like part of the inner ear found in mammals, the cochlear duct is a long blind tube with a slight curvature[12].

There is some debate regarding when hearing emerges in the avian embryo, with studies defining the avian embryo's ability to hear beginning on embryonic day 10 (E10) and embryonic day 12 (E12) [17][18]. The cochlea may be seen in a developing embryo as early as day E3. By day E9, the cochlear duct has been constructed and all subsequent days of embryonic development are used for an increase in overall size of the inner ear[12]. **Figure 1**, licensed from the Standard Atlas of the Gross Anatomy of the developing Inner Ear of the Chicken, shows the anatomical development of the avian inner ear.

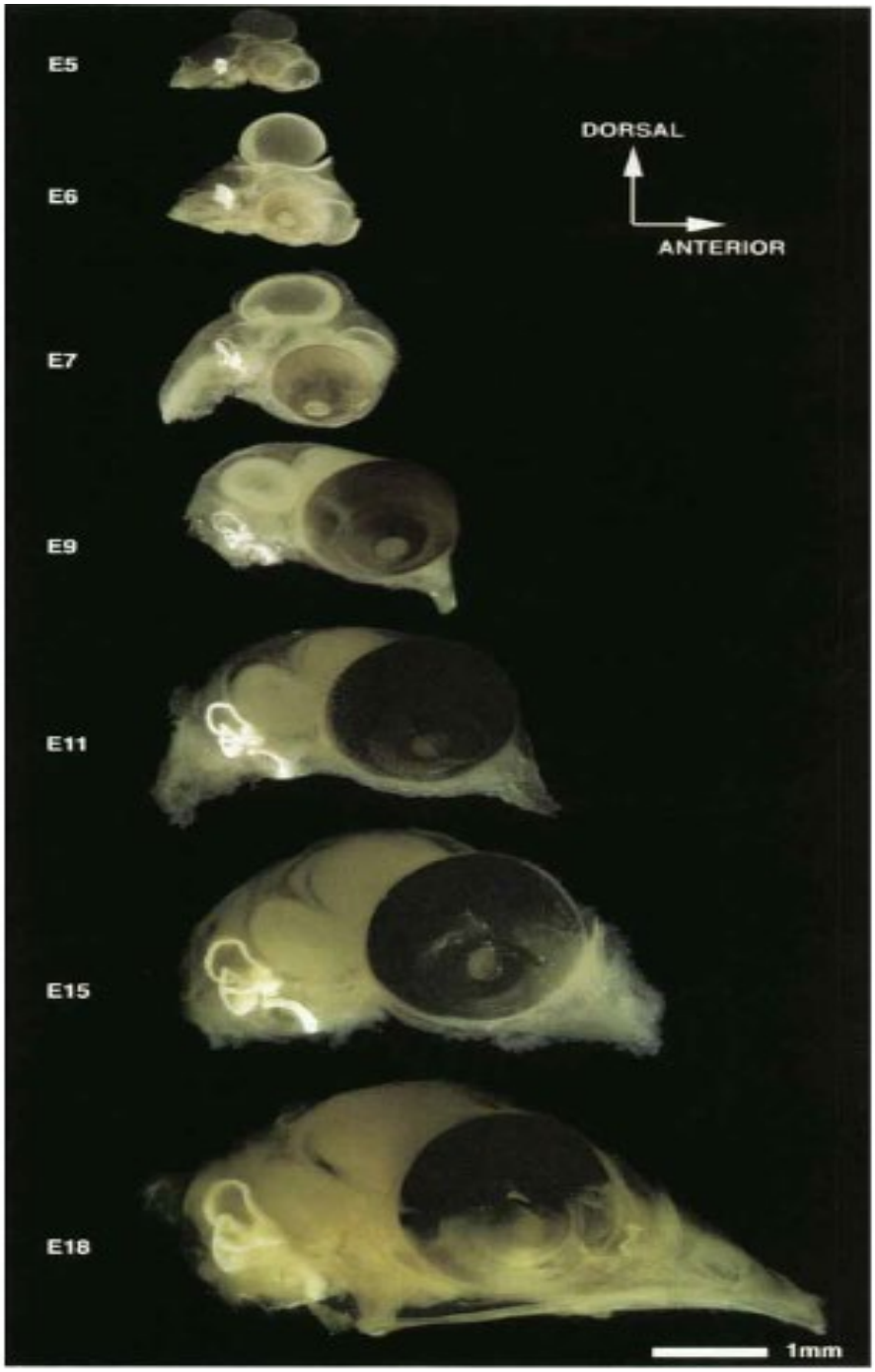

Figure 1. Growth chart of avian cochlea starting from embryonic day 5 (E5) to embryonic day 18 (E18). Reprinted from Standard Atlas of the Gross Anatomy of the Developing Inner Ear of the Chicken [12] and used with permission.

Similarly, **Figure 2** is a growth chart of the inner ear where you can see the overall shape does not change much after day E9.

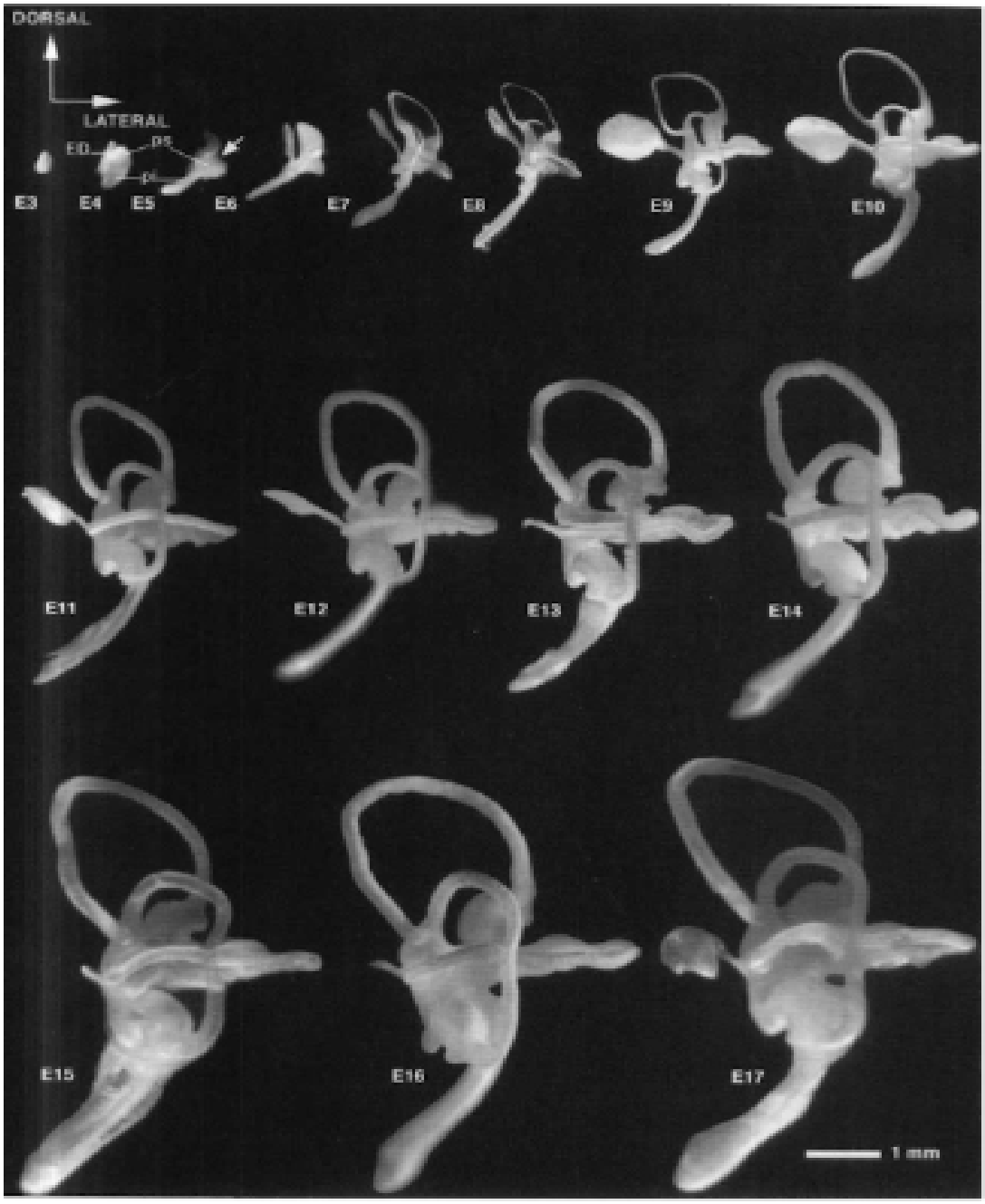

Figure 2. Growth chart of the avian inner ear from embryonic day 3 (E3) to embryonic day 17 (E17). Reprinted from Standard Atlas of the Gross Anatomy of the Developing Inner Ear of the Chicken [12] and used with permission.

Inside the cochlea there are two types of cells, hair cells (HC) and supporting cells (SC). Contrary to humans, chickens have the ability to regrow lost HCs inside the inner ear to regain hearing loss[19][20]. HCs, identified by the population of stereocilia sprouting from an otherwise smooth surface, are separated by a ridge of microvilli. Thin sections reveal that all of these microvilli extend from supporting cells that surround and separate each hair cell [21].We find that the length, number, width, and distribution of the stereocilia on each hair cell are predetermined[22]. These factors differ based on physical location on the cochlea and developmental stage. The superior side of the cochlea is home to longer hair cells, whereas the inferior side houses the shorter hair cells[21]. There are two types of hair cells, tall hair cells (THC) and short hair cells (SHC). The THC are primarily found over the fibrocartilaginous plate (FC), whereas the SHC are developed over the basilar membrane (BM)[18][21]. THCs and SHCs are developed in a staircase like pattern.

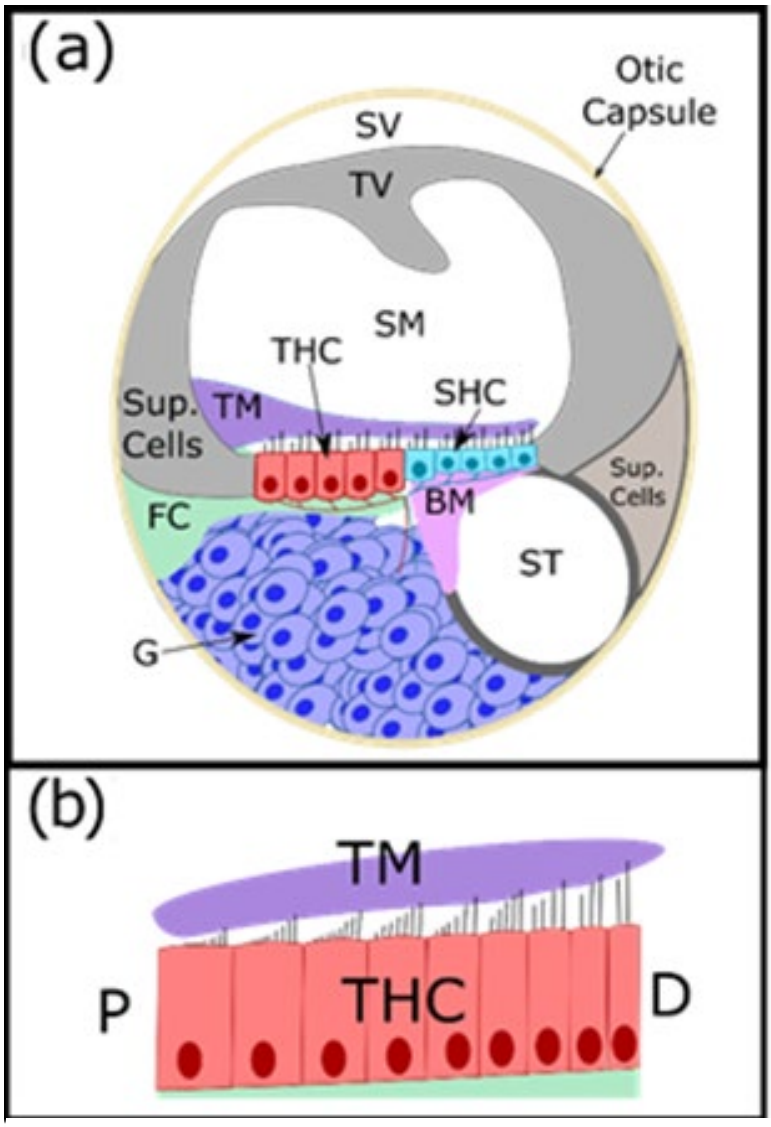

Figure 3. (a) Artistic rendering of avian cochlear duct showing main components. **(b)**Staircase like innervation of the hair cells into the tectorial membrane

Bundles of actin filaments precisely regulate the length and stiffness of the stereocilia. Actin is the most commonly encountered protein in nonmuscle cells, where it can account for more than 15% of the total protein of the cell[22]. The HCs are arranged in hexagonal bundles within the cochlea and convert mechanical vibrations into the electrical signals required for auditory sensation[6]. Studies show that the tonotopic pattern of these bundles may be directly correlated with frequency coding in the cochlear duct[23]. While the stiffness of these bundles strongly influences mechanotransduction, the influence on the vibratory response of the cochlear partition is unclear. Reducing bundle stiffness is shown to decrease high frequency extent and sharpen the tuning of vibratory responses[6]. The stereocilia first appear on the distal end of the cochlea on days E6 or E7. The true differentiation in pattern occurs on day E9 or E10. This is when you can see an elongation occurring in the overall shape of the cochlea as well as the tonotopic pattern of the hair cells[18]. The number of HCs present on day E10, is the total number of HCs the cochlea will have. This is roughly 10,405± 529 hair cells[18][24]. By day E10 the hexagonal shape is fully formed and the overall pattern of the stereocilia does not change tremendously. By day E13, the stereocilia at the foot of the staircase can be seen reabsorbing into the tissue below and the final shape is recognized[18].

When a sound is sent into the cochlea, a number of events occur in order to allow the sound to be processed by the brain. A sound wave is collected by the outer ear and directed to the tympanic membrane. The tympanic membrane is mechanically coupled to the inner ear through structures of the middle ear[25]. In avian species, the middle ear is a single cartilaginous structure known as the columella[26]. The footplate of the columella is mechanically coupled to the oval window of the cochlear duct, providing the mechanical stimulation entering the inner ear. Sound is then sent to the scala tympani (ST) which separates the cochlear duct from the

basilar membrane (BM). Here is the first transduction of air that causes vibration. This vibration then moves up the BM toward the fibrocartilaginous plate. The FC rests on top of cochlear nerve ganglion cells. The THCs situated on the FC are tall enough to extend themselves into the lower edge of the tectorial membrane (TM). Then using afferent neurons innervated in THCs, the sound causes movement in the TM. Now, the scala media (SM) is responsible for converting mechanical forces into electrical impulses. The membrane of the teculum vestibular (TV) is then responsible for transporting the electrical impulses to the brain. [25][27][28][29][30][31][32]

2.1 OCT and OCV

In time domain optical coherence tomography, light is sent from a source toward a beam splitter where it is divided evenly. Half of the light is sent toward the sample and the other half is sent toward a moving mirror. The light reflects off the sample and the mirror and is recombined by the beam splitter and sent toward the detector. If the pathlengths match within a coherence length, interference will occur. OCT measures the intensity of the interference[33].

In a spectral domain optical coherence tomography (SDOCT) system, the detector is replaced with a spectrometer, the reference arm and mirror are stationary, the acquisition time is shorter, and there is a greater sensitivity. SDOCT is an interferometric technique that provides depth-resolved tissue structure information including the magnitude and delay of the back-scattered light by spectral analysis of the interference fringe pattern[34]. In SDOCT, the interference signal between the reference light and the scattering light from within a sample is spectrally resolved by a linear array detector, which is then Fourier transformed to obtain the amplitudes and phases of the light reflected from the sample as a function of depth[35].

3.3 Mathematical Treatment of OCV

Math for OCV begins with the same math as a standard OCT system. The spectral interferogram can be written as [33]:

$$\boldsymbol{I(k)\alpha\ Re\{\iint S(k)r(x,z)\ \exp\left(4ln2\left(\frac{x^2}{w_0}\right)\right)\exp(-i2kz)dxdz\}} \quad \textbf{(1)}$$

The equation states that the intensity I, a function of k=2π/ λ (λ= wavelength), is proportional to the real part, Re{}, of the following double integrals. S(k) is the source power of spectral density, another function of k, multiplied by the backscattering coefficient of the sample, r(x,z), where (x,z) denote the coordinate of the reference frame fixed to the sample. This is all multiplied by two different exponentials containing w_0, the full width at half maximum of the beam's intensity profile. Equation (1) can be rewritten as an equivalent sinusoidal function:

$$\mathbf{I(k)} \propto \mathbf{S(k)\Sigma j}\sqrt{\boldsymbol{R_{sj}R_r}}\boldsymbol{cos\{2nk\Delta z_j + 2nk_0dz_j\}} \quad \textbf{(2)}$$

S(k) becomes the power spectrum of the light source rather than the spectral density. The reflectivity of the sample is now R_{sj}, at the j^{th} depth, and R_r is the reflectivity of the reference arm. The refractive index between the reference and sample arm reflectors is labeled n, and k is the wavenumber with k_0 being the center wavenumber. Δz_j is the distance between the reference reflector and the j^{th} reflector in the sample and is defined as the full width at half maximum of the spectrum source. Lastly, dz_j is the sub resolution displacements of the j^{th} reflector in the sample arm. Also known as the phase shift. A few observations may be made from equation (2) regarding OCT. First, the reference arm has two roles in the system: to serve as a source of interference and to amplify the signal generated from the significantly weaker sample arm reflections. Next, when working with a digital system, the sampling of the spectrum in k will define our Nyquist limited imagine depth[36]. In addition, it may be seen that the depth dependent signal of the cosine function acts as a phase encoded carrier wave for subresolution

displacements of the sample. This phase encoding is key to the effective extraction of vibrational motion in OCV.

The raw data acquired from the spectrometer shows the intensity, of a pattern of light, as a function of wavelengths λ. An interpolation is done to find the wave number, k, (seen in equation (2)). Then we take the inverse Fourier transform of (2) which yields a complex signal in the z-space:

$$\boldsymbol{I(x) \propto \frac{1}{2}\gamma(z)\otimes\Sigma_i\sqrt{R_{si}R_r}\delta[z \pm 2n\Delta z]exp \pm 2njk_0dz} \quad \textbf{(3)}$$

$\gamma(z)$, the coherence function, is the Fourier transform of S(k), $\otimes$ is the convolution operator, and δ is the Dirac delta function. The position in depth within the sample is denoted by z. For any given Δz, the phase of the signal is a linear function of dz and the change in phase can be plotted over time. The following equation can be used to convert the phase of the interferogram to displacement [37]:

$$\boldsymbol{dz(2n\Delta z, t) = \frac{1}{2nk_0}(< I(2n\Delta z, t) - < I(2n\Delta z, t_0))} \quad \textbf{(4)}$$

As stated previously, these Fourier Transforms obtain both the amplitudes and phases of the light within the sample. Generally, with OCT the samples are static therefore the phases are fixed. If translation occurs within the sample at time t with the distance Δd(t) during the time interval τ between two successive scans, it will induce a change in the measured phase of light given by:

$$\boldsymbol{\Delta\phi(z,t) = 2nk\Delta d(t)} \quad \textbf{(5)}$$

If you calculate this phase difference at each depth z, you can determine the axial displacement of the sample[35].

$$\boldsymbol{\Delta d(z,t) = \Delta\phi(z,t)\lambda(4\pi n)^{-1}} \quad \textbf{(6)}$$

CHAPTER 3-MATERIALS AND METHODS

3.1 Instrumentation

Below is a list of all instruments used in the project with various specifications as follows:

- Fertilized White Leghorn eggs
- Scalpel
- Tweezers
- Gel lined Dish
- Super Luminescent Diode (SLD) with 930nm, 30nm bandwidth and 20mW optical power, forward current of 150mA, forward voltage 2.5V
- Cobra-S Spectrometer with a 60 nm bandwidth, 2048 pixels, centered at 930 nm
- Computer Interface
- Function Generator
- 75-25 Optical Beam Splitter
- Optical Circulator
- Voice Coil Scanning Mirror
- Reference Mirror

3.2 Embryo Preparation

Embryos were stored at 13°C for up to 1 month prior to incubation. At the onset of the study, eggs were incubated at 30°C, for 10 days to 13 days. An automatic turner was used to rotate the eggs at a rate of one rotation every twelve hours. Humidity in the incubator was kept between 70% and 90% throughout incubation. Immediately prior to dissection and imaging, embryos were sacrificed via decapitation.

3.3 OCT imaging and OCV

There are three different scans collected from the raw data. An A scan is a one axis scan used to collect information in only a specified axis. An M scan is a collection of A scans over time. This is helpful with vibrometry because you can play a sound and watch one point over time. A B scan is a two-axis scan collecting data in two axes; it is a combination of two A scans. A volume scan is a collection of B scans. This adds depth to the image as it is a collection of slices through a sample[33][38][39][40].

In order to obtain the final vibrational motion at each frequency, there are several steps taken. The math of each step is detailed in the previous chapter. We look at each individual point in the sample and collect thousands of A scans, generating an M scan. The raw data of each image gives us the amplitude of the intensity at each wave number. Then a Fourier Transform is performed, and the processed data then reveals the magnitude at each depth. The depth profile generates an image with reflectivity based on the hardness of the tissue in the sample. Dark indicates a fluid or air-filled cavity whereas bone or harder tissue reflects as very bright white.

Figure 4 below is an interpretation of how the depth profile is created.

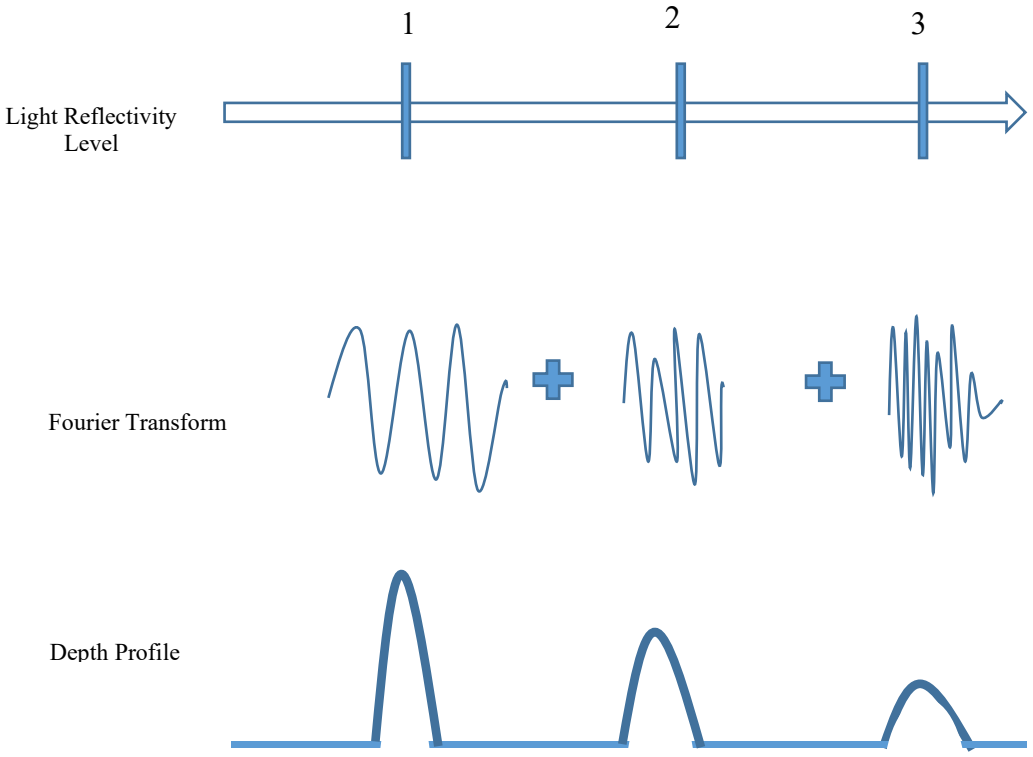

Figure 4. Interpretation of mathematic manipulatio
of OCT.

Now a sound is played, and the phase profile can be extracted over time. If our hypothesis is correct, we should see a perfect sine wave in this profile. Then one last Fourier Transform is performed in order to get our final amount of vibrational motion at each specified frequency. These steps are repeated for every individual point in sample and at each specified frequency.

Figure 5 below depicts a schematic of our current OCT system. The design is centered around the optical circulator (OF-LINK) to enable the use of a 75-25 fiber optic beam splitter (ThorLabs) for more optimized signal collection. Light enters port one of the circulator, from the super luminescent diode source (930 nm, 120 nm bandwidth, ThorLabs) and leaves through port two into the 75-25 fiber optic beam splitter. Next, 25% of light is directed to the reference arm and

75% of the light is directed to the sample arm. The sample arm utilizes a voice coil scanning mirror (Optics in Motion) to steer the beam laterally across the sample. Back scattered light, from both the sample and reference arms, is recombined in the beam splitter and 75% of the backscattered light is returned to port 2 of the circulator. Light entering port 2, leaves through port 3 and is directed into the detector. In this case, we are utilizing SDOCT so our detector is a spectrometer centered at 930 nm with a 60 nm bandwidth (Wasatch Photonics).

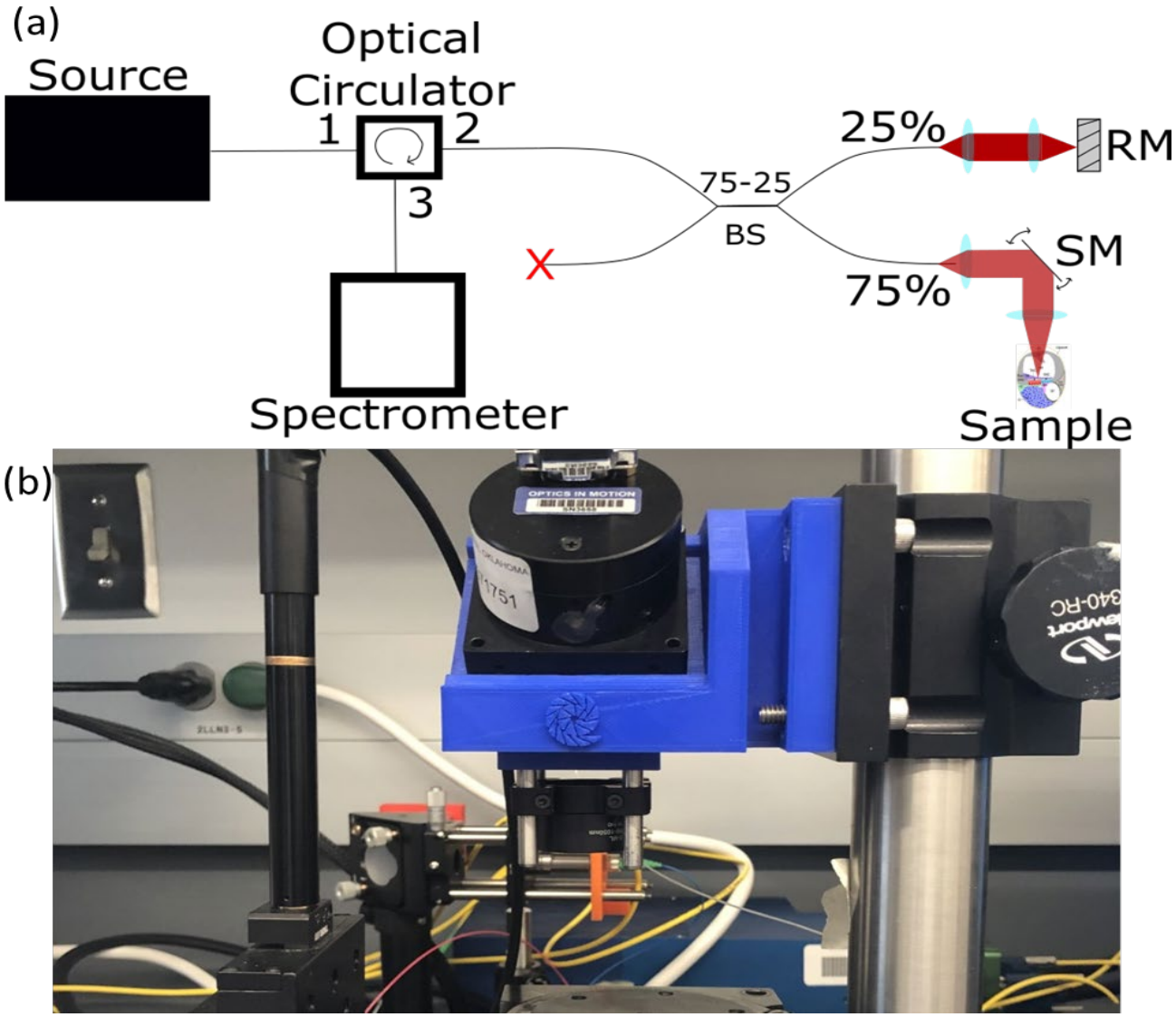

Figure 5. (a) Schematic drawing of the OCT system showing major components. SM is scan mirror and RM is reference mirror. **(b)** Image of actual system showing the small form factor and large working distance of the system.

3.4 Experimental Procedure for Pure Tone Audiometry

A custom LabVIEW software was utilized to synchronize audio output with signal collection. This software generated and output a pure tone audio sample to an amplified speaker in order to vibrate the sample. From literature, it was determined that frequencies above 2,200Hz were unable to be recognized by the embryo [17]. In addition, due to environmental pink noise, we were unable to isolate signal from sound frequencies below 1000Hz. Therefore, we chose the frequencies of 1,000Hz, 1,500Hz, and 2,000Hz. This allowed for a reasonable range of data that was visible in the obtained images. In addition, varying sound pressure levels (SPL) of 0dB, 40dB, 60dB, and 90dB were utilized to map out the linear gain of the cochlear duct.

CHAPTER 4-RESULTS & DISCUSSION

4.1 Development of Embryo Dissection Procedure

To accomplish the research, a repeatable procedure to access the avian cochlear duct, of the developing embryo, had to be established. The embryo's head was placed in a sterile gel bottomed dish and pins were used to orient the head. From the literature, it was determined that the nasoocciptital axis of the head was to be adjusted nearly 30° off the vertical to the right, in order to reach the cochlea[17]. For ease of access, the eyeball was removed and discarded on the side we were working on. A scalpel and a pair of tweezers was then used to slowly peel back the tissue over the cochlea in order to maximize the image under the OCT. This procedure had to be modified to ensure the same angle of axis throughout development of the cochlear duct. In embryos older than E11, the lower jaw of the beak was removed to provide access to the cochlear duct region. To ensure consistency between samples, the specimen was then placed under the system and a 3-D dataset was captured using OCT. The orientation of the cochlea was found using the very distinguishable three-layer structure and is compared to our baseline model.

4.2 Preliminary Study of the Developing Cochlear Duct

We have completed a preliminary study of the changes in the mechanical motion within the developing cochlear duct. The cochlear duct of developing chicken embryos age E12 and E13 of embryological development were imaged using OCT in **Figure 6**. The yellow region is the tectorial membrane (TM) which had measured a vibrational motion of 17. 6 ± 2.4 nm. The orange region is the basilar membrane (BM) which measured a vibrational motion of 25.2 ± 4.5 nm. Due to an unfortunate glitch in our software, this segmentation was performed manually during post processing instead of using our real time processing functions.

For our experiment we used a range of 1000Hz to 2000Hz and chose the sound pressure levels of 0 dB, 40 dB, 60 dB, and 90 dB in coordination with literature[17]. The 0dB signal was

used to normalize our results. The region of the cochlear duct with the greatest response to 2000 Hz pure tone signal was identified in both the E12 and E13 embryo sample and the values of mechanical motion of the basilar membrane and tectorial membrane were compared. The results are as seen in **Figure 7**.

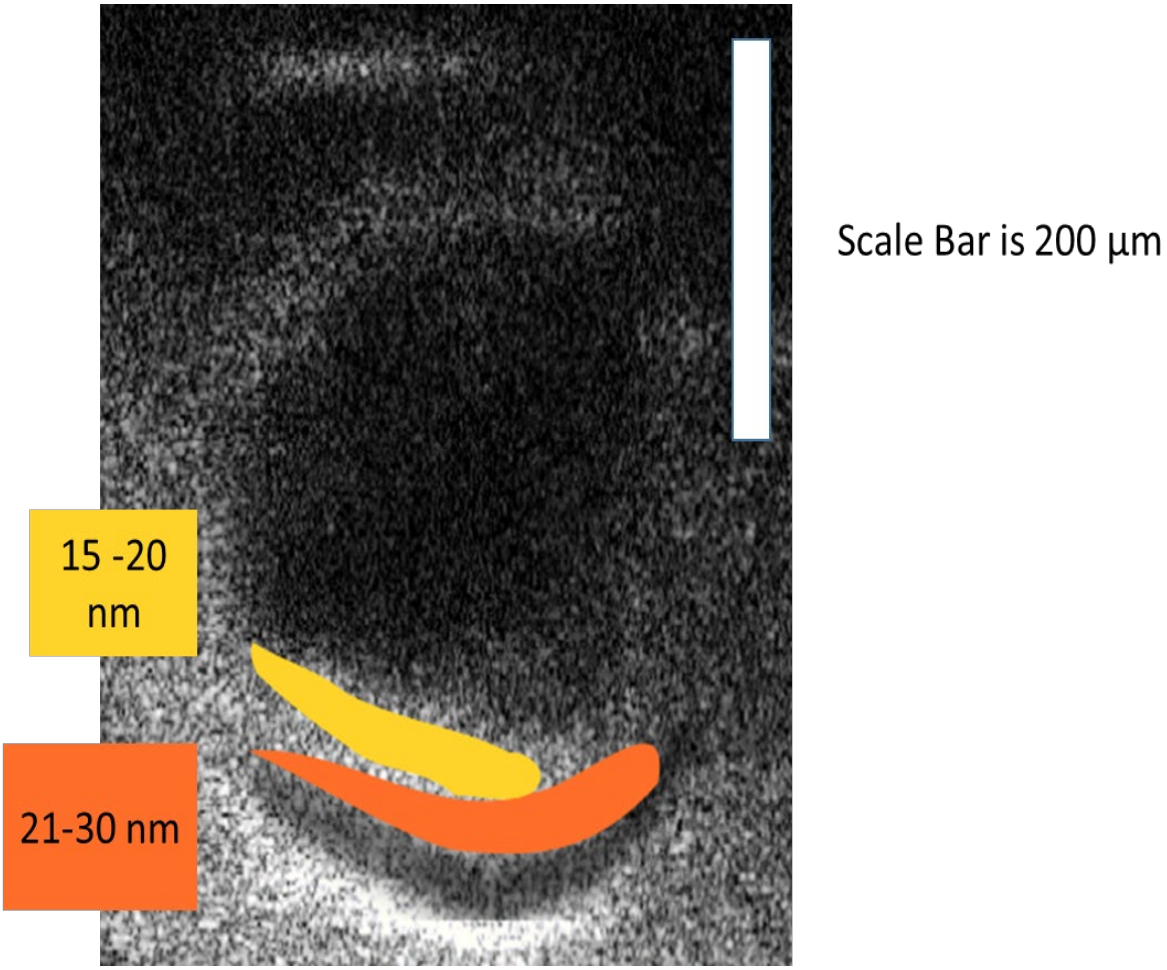

Figure 6. An OCT image of the organ of Corti captured with our OCV system. It should be noted that this image has been flipped from its initial orientation.

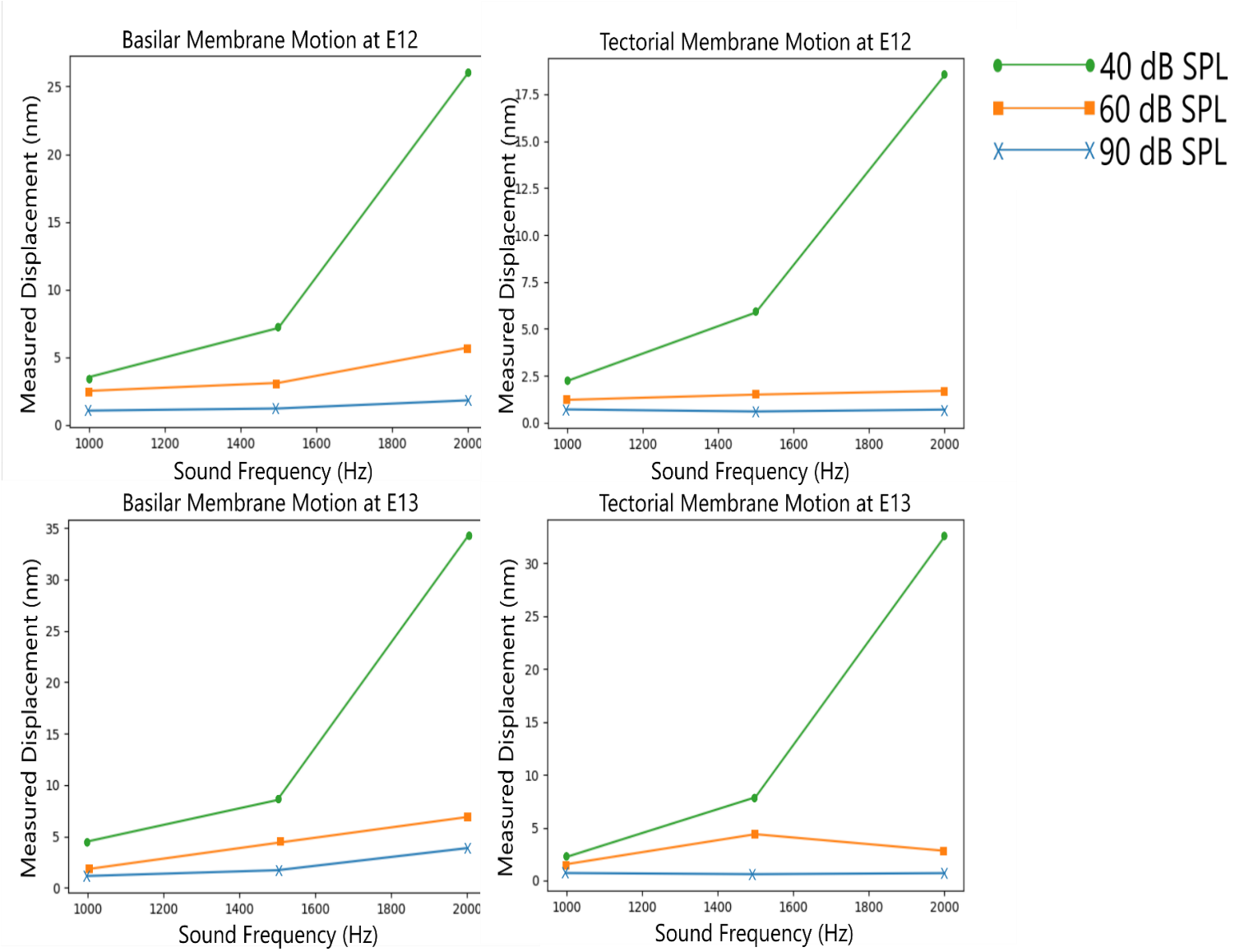

Figure 7. Results of vibrational motion experiment on the TM and BM.

4.3 Discussion

There are several key challenges for accessing the same region of the cochlear duct at varying developmental stages. The most pertinent being the growth of the cochlear duct that is occurring between days E10 and E13 of development. During this time period the cochlear duct almost doubles in size. Therefore, while we have developed an effective procedure for obtaining access to the cochlear duct from a consistent geometry, as it is difficult to directly compare motion of the varying regions of the cochlear duct between developmental ages. In addition, our

initial results from the cochlear duct were normalized to the motion of the cochlea in the absence of auditory stimuli. Instead, it would be better to normalize our signal to the motion of the oval window. This will remove any artifacts that arise due to the changes in the middle ear occurring simultaneously during development. Depending on future results, moving forward it may be pertinent to remove the columella and directly couple a piezoelectric transducer to the oval window of the cochlear duct.

It is also important to emphasize that no conclusions may be drawn from this preliminary data, as we need to repeat this experiment and verify statistical significance of our results. From the literature, we believe a sample size of 3-4 embryos at each developmental stage will be enough to ensure significance of our results; however, it is impossible to fully estimate this number without more data on the variation between developmental stages of the embryo. Should we see large variations in our results, we would recommend verifying the developmental stage of the cochlear duct using scanning electron microscopy.

CHAPTER 4-CONCLUSION

We have determined an experimental procedure for a repeatable access of the avian cochlear duct for imaging via OCV. In addition, we have repeated a preliminary study of the changes in mechanical motion of the avian cochlear duct. This study is very limited in that it has only one individual per age group. While this experiment needs much more repeatability in order to verify early data, it provides a hopeful insight into the changes in mechanical motion of the cochlear duct. There are many other frequencies and sound pressure levels that need to be tested. I recommend frequencies from 1000 Hz to 2,500 Hz in 100 Hz steps in order to verify the early results we have seen. I also recommend that future research should include a larger range of sound pressure levels. If we can determine repeatable results, work can be made toward rendering a mechanical model of the coupling inside the inner ear of avian chicken embryos.

REFERENCES

[1] "Hearing loss | NHS inform." https://www.nhsinform.scot/illnesses-and-conditions/ears-nose-and-throat/hearing-loss (accessed Mar. 04, 2020).

[2] J. S. Oghalai, "Hearing and Hair Cells." Accessed: Mar. 13, 2020. [Online]. Available: http://www.neurophys.wisc.edu/.

[3] "Deafness and hearing loss." https://www.who.int/news-room/fact-sheets/detail/deafness-and-hearing-loss (accessed Mar. 04, 2020).

[4] "Hearing Aids | NIDCD." https://www.nidcd.nih.gov/health/hearing-aids (accessed Mar. 13, 2020).

[5] N. C. Lin, C. P. Hendon, and E. S. Olson, "Signal competition in optical coherence tomography and its relevance for cochlear vibrometry," *The Journal of the Acoustical Society of America*, vol. 141, no. 1, pp. 395–405, Jan. 2017, doi: 10.1121/1.4973867.

[6] J. B. Dewey, A. Xia, U. Müller, I. A. Belyantseva, B. E. Applegate, and J. S. Oghalai, "Mammalian Auditory Hair Cell Bundle Stiffness Affects Frequency Tuning by Increasing Coupling along the Length of the Cochlea," *Cell Reports*, vol. 23, no. 10, pp. 2915–2927, Jun. 2018, doi: 10.1016/j.celrep.2018.05.024.

[7] A. Xia, X. Liu, P. D. Raphael, B. E. Applegate, and J. S. Oghalai, "Hair cell force generation does not amplify or tune vibrations within the chicken basilar papilla," *Nature Communications*, vol. 7, p. 13133, Oct. 2016, doi: 10.1038/ncomms13133.

[8] C. Guo *et al.*, "Image-guided vibrometry system integrated with spectral- and time-domain optical coherence tomography," *Applied Optics*, vol. 58, no. 7, p. 1606, Mar. 2019, doi: 10.1364/ao.58.001606.

[9] Y. Chen, X. Guan, T. Zhang, and R. Z. Gan, "Measurement of Basilar Membrane Motion During Round Window Stimulation in Guinea Pigs," *JARO - Journal of the Association for Research in Otolaryngology*, vol. 15, no. 6, pp. 933–943, Nov. 2014, doi: 10.1007/s10162-014-0477-5.

[10] X. Wang, X. Guan, M. Pineda, and R. Z. Gan, "Motion of tympanic membrane in guinea pig otitis media model measured by scanning laser Doppler vibrometry," *Hearing Research*, vol. 339, pp. 184–194, Sep. 2016, doi: 10.1016/j.heares.2016.07.015.

[11] W. Dong, A. Xia, P. D. Raphael, S. Puria, B. Applegate, and J. S. Oghalai, "Organ of Corti vibration within the intact gerbil cochlea measured by volumetric optical coherence tomography and vibrometry," *Journal of Neurophysiology*, vol. 120, no. 6, pp. 2847–2857, Dec. 2018, doi: 10.1152/jn.00702.2017.

[12] J. P. Bissonnette and D. M. Fekete, "Standard atlas of the gross anatomy of the developing inner ear of the chicken," *Journal of Comparative Neurology*, vol. 368, no. 4, pp. 620–630, May 1996, doi: 10.1002/(SICI)1096-9861(19960513)368:4<620::AID-CNE12>3.0.CO;2-L.

[13] R. Romand, "Modification of tonotopic representation in the auditory system during development," *Progress in Neurobiology*, vol. 51, no. 1. Pergamon, pp. 1–17, Jan. 01, 1997, doi: 10.1016/S0301-0082(96)00043-3.

[14] R. Fettiplace and P. A. Fuchs, "MECHANISMS OF HAIR CELL TUNING," 1999. Accessed: Apr. 19, 2020. [Online]. Available: www.annualreviews.org.

[15] M. R. Stinson and S. M. Khanna, "Sound propagation in the ear canal and coupling to the eardrum, with measurements on model systems," *Journal of the Acoustical Society of America*, vol. 85, no. 6, pp. 2481–2491, Jun. 1989, doi: 10.1121/1.397743.

[16] "The Otolith Organs: The Utricle and Sacculus - Neuroscience - NCBI Bookshelf." https://www.ncbi.nlm.nih.gov/books/NBK10792/ (accessed Mar. 13, 2020).
[17] T. A. Jones, S. M. Jones, and K. C. Paggett, "Emergence of Hearing in the Chicken Embryo," *Journal of Neurophysiology*, vol. 96, no. 1, pp. 128–141, Jul. 2006, doi: 10.1152/jn.00599.2005.
[18] L. G. Tilney, M. S. Tilney, J. S. Saunders, and D. J. DeRosier, "Actin filaments, stereocilia, and hair cells of the bird cochlea. III. The development and differentiation of hair cells and stereocilia," *Developmental Biology*, vol. 116, no. 1, pp. 100–118, Jul. 1986, doi: 10.1016/0012-1606(86)90047-3.
[19] H. R. Brignull, D. W. Raible, and J. S. Stone, "Feathers and fins: Non-mammalian models for hair cell regeneration," *Brain Research*, vol. 1277. NIH Public Access, pp. 12–23, Jun. 24, 2009, doi: 10.1016/j.brainres.2009.02.028.
[20] E. W. Rubel, S. A. Furrer, and J. S. Stone, "A brief history of hair cell regeneration research and speculations on the future," *Hearing Research*, vol. 297. NIH Public Access, pp. 42–51, Mar. 2013, doi: 10.1016/j.heares.2012.12.014.
[21] L. G. Tilney and J. C. Saunders, "Actin Filaments, Stereocilia, and Hair Cells of the Bird Cochlea I. Length, Number, Width, and Distribution of Stereocilia of Each Hair Cell Are Related to the Position of the Hair Cell on the Cochlea," 1983. Accessed: Apr. 19, 2020. [Online].
[22] L. G. Tilney and J. C. Saunders, "Actin filaments, stereocilia, and hair cells of the bird cochlea I. Length, number, width, and distribution of stereocilia of each hair cell are related to the position of the hair cell on the cochlea," *Journal of Cell Biology*, vol. 96, no. 3, pp. 807–821, Mar. 1983, doi: 10.1083/jcb.96.3.807.
[23] T. F. Weiss, M. J. Mulroy, R. G. Turner, and C. L. Pike, "Tuning of single fibers in the cochlear nerve of the alligator lizard: Relation to receptor morphology," *Brain Research*, vol. 115, no. 1, pp. 71–90, Oct. 1976, doi: 10.1016/0006-8993(76)90823-4.
[24] L. G. Tilney, M. S. Tilney, and D. J. Derosier, "ACTIN FILAMENTS, STEREOCILIA, AND HAIR CELLS: How Cells Count and Measure," 1992. Accessed: Apr. 19, 2020. [Online]. Available: www.annualreviews.org.
[25] G. Volandri, F. di Puccio, P. Forte, and C. Carmignani, "Biomechanics of the tympanic membrane," *Journal of Biomechanics*, vol. 44, no. 7. Elsevier, pp. 1219–1236, Apr. 29, 2011, doi: 10.1016/j.jbiomech.2010.12.023.
[26] J. L. Wood, A. J. Hughes, K. J. Mercer, and S. C. Chapman, "Analysis of chick (Gallus gallus) middle ear columella formation," *BMC Dev Biol*, vol. 10, p. 16, 2010, doi: 10.1186/1471-213X-10-16 1471-213X-10-16 [pii].
[27] M. Mathews, "The Ear and How It Works." Accessed: Apr. 19, 2020. [Online].
[28] A. Forge and T. Wright, "The molecular architecture of the inner ear," 2002. Accessed: Apr. 19, 2020. [Online]. Available: https://academic.oup.com/bmb/article-abstract/63/1/5/377516.
[29] W. E. Brownell, "HOW THE EAR WORKS - NATURE'S SOLUTIONS FOR LISTENING," *The Volta review*, vol. 99, no. 5, p. 9, 1997, Accessed: Apr. 19, 2020. [Online].
[30] T. Cheng, C. Dai, and R. Z. Gan, "Viscoelastic properties of human tympanic membrane," *Annals of Biomedical Engineering*, vol. 35, no. 2, pp. 305–314, Feb. 2007, doi: 10.1007/s10439-006-9227-0.

[31] E. W. Abel and R. M. Lord, “A finite-element model for evaluation of middle ear mechanics,” in *Annual International Conference of the IEEE Engineering in Medicine and Biology - Proceedings*, 2001, vol. 2, pp. 2110–2112, doi: 10.1109/iembs.2001.1020651.

[32] R. Z. Gan, T. Cheng, C. Dai, F. Yang, and M. W. Wood, “Finite element modeling of sound transmission with perforations of tympanic membrane,” *The Journal of the Acoustical Society of America*, vol. 126, no. 1, pp. 243–253, Jul. 2009, doi: 10.1121/1.3129129.

[33] D. Huang *et al.*, “Optical coherence tomography,” *Science*, vol. 254, no. 5035, pp. 1178–1181, 1991, doi: 10.1126/science.1957169.

[34] Z. Yaqoob, J. Wu, and C. Yang, “Spectral domain optical coherence tomography: a better OCT imaging strategy.,” *BioTechniques*, vol. 39, no. 6 Suppl. Future Science Ltd London, UK , May 30, 2005, doi: 10.2144/000112090.

[35] R. K. Wang, Z. Ma, and S. J. Kirkpatrick, “Tissue Doppler optical coherence elastography for real time strain rate and strain mapping of soft tissue,” *Applied Physics Letters*, vol. 89, no. 14, 2006, doi: 10.1063/1.2357854.

[36] I. Gurov, M. Taratin, and A. Zakharov, “High-speed Signal Evaluation in Optical Coherence Tomography Based on Sub-Nyquist Sampling and Kalman Filtering Method,” in *AIP Conference Proceedings*, Oct. 2006, vol. 860, no. 1, pp. 146–150, doi: 10.1063/1.2361215.

[37] H. C. Hendargo, A. K. Ellerbee, and J. A. Izatt, “Spectral domain phase microscopy,” *Springer Series in Surface Sciences*, vol. 46, no. 1, pp. 199–228, 2011, doi: 10.1007/978-3-642-15813-1_8.

[38] Z. Yaqoob, J. Wu, and C. Yang, “Spectral domain optical coherence tomography: a better OCT imaging strategy.,” *BioTechniques*, vol. 39, no. 6 Suppl. Future Science Ltd London, UK , May 30, 2005, doi: 10.2144/000112090.

[39] M. F. Kraus *et al.*, “Motion correction in optical coherence tomography volumes on a per A-scan basis using orthogonal scan patterns,” *Biomedical Optics Express*, vol. 3, no. 6, p. 1182, Jun. 2012, doi: 10.1364/boe.3.001182.

[40] R. D. Ferguson, D. X. Hammer, L. A. Paunescu, S. Beaton, and J. S. Schuman, “Tracking optical coherence tomography,” *Optics Letters*, vol. 29, no. 18, p. 2139, Sep. 2004, doi: 10.1364/ol.29.002139.

APPENDIX A

Thank you for your order!

Dear Kristen Stromsodt,

Thank you for placing your order through Copyright Clearance Center's RightsLink® service.

Order Summary

Licensee:	Kristen Stromsodt
Order Date:	Mar 19, 2020
Order Number:	4792320470693
Publication:	Journal of Comparative Neurology
Title:	Standard atlas of the gross anatomy of the developing inner ear of the chicken
Type of Use:	Dissertation/Thesis
Order Total:	0.00 USD

View or print complete details of your order and the publisher's terms and conditions.

Sincerely,

Copyright Clearance Center

Tel: +1-855-239-3415 / +1-978-646-2777
customercare@copyright.com
https://myaccount.copyright.com

Copyright Clearance Center RightsLink®